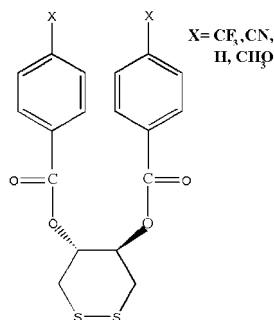


so-called Kelvin probe that is used to measure the CPD between free, modified Au surfaces and an unmodified one. Table 1 shows the CPD values as a function of the phenyl part's dipole [34]. The work function of Au can be changed over a potential range of 1.2 V. The dipole effect is nonlinear because the molecules have somewhat different coverages and average orientations (tilt) on the surface. For further details on the characterization of these molecularly modified surfaces, the reader is referred to the literature [20].



Scheme 1.

Table 1. Effect of molecular dipole on the work function of gold. The results for each molecule are an average of 5 experiments.

Benzene substituent	Dipole moment of substituted phenyl [34] [Debye]	Δ CPD (Au) – (modified Au) [mV]	Error [mV]
CH ₃ O	-1.25	-484	2
H	0	-427	6
CN	3.9	420	27
CF ₃	2.58	732	14

The Au contacts are deposited on the Si surfaces using a slight modification of the LOFO technique [1,35]. The Au leaves are made to float, for a period of 16–24 h in a closed Teflon vial, on an acetonitrile solution of the disulfide molecules. Prior to the 'float-on' step the solution is changed, by means of a small pipette, to a clean acetonitrile solution. Subsequently, a Si substrate (covered with an oxide layer, grown under controlled conditions, 10–15 Å thick, as measured by ellipsometry) is immersed into the solution to complete the 'float-on'. In this study <100> Si wafers were used (Virginia Semiconductor Inc), that were P-doped to $\sim 10^{17}$ cm⁻³. Between 5 and 7 modified diodes were made with each type of molecule. *I*-*V* curves were measured under vacuum (10 mtorr) in a temperature range of 160–300 K. Each diode was cycled 2–3 times prior to the actual measurement in order to test its stability and steady-state behavior.

Received: September 20, 2000
Final version: November 14, 2000

[1] A. Vilan, A. Shanzer, D. Cahen, *Nature* **2000**, 404, 166.
 [2] J. Hoelzel, F. K. Schulte, H. Wagner, *Solid State Surface Physics*, Springer, Berlin **1979**.
 [3] H. Ishii, K. Sugiyama, E. Ito, K. Seki, *Adv. Mater.* **1999**, 11, 605.
 [4] C. B. Duke, C. Mailhot, *J. Vac. Sci. Technol. B* **1985**, 3, 1170.
 [5] C. Berthod, N. Binggeli, A. Baldereschi, *J. Vac. Sci. Technol. B* **2000**, 18, 2114.
 [6] C. Marinelli, L. Sorba, M. Lazzarino, D. Kumar, E. Pelucchi, B. H. Müller, D. Orani, S. Rubini, A. Franciosi, S. De Franceschi, F. Beltram, *J. Vac. Sci. Technol. B* **2000**, 18, 2119.
 [7] J. Ivanco, H. Kobayashi, J. Almeida, G. Margaritondo, *J. Appl. Phys.* **2000**, 87, 795.
 [8] C. Ohler, C. Daniels, A. Förster, H. Lüth, *Phys. Rev. B: Condens. Matter* **1998**, 58, 7864.
 [9] J. Almeida, C. Coluzza, T. dell'Orto, G. Margaritondo, A. Terrasi, J. Ivanco, *J. Appl. Phys.* **1997**, 81, 292.
 [10] L. Sorba, S. Yildirim, M. Lazzarino, A. Franciosi, D. Chiola, F. Beltram, *Appl. Phys. Lett.* **1996**, 69, 1927.
 [11] C. Berthod, N. Binggeli, A. Baldereschi, *Europhys. Lett.* **1996**, 36, 67.
 [12] J. Tersoff, *Phys. Rev. Lett.* **1984**, 52, 465.
 [13] I. H. Campbell, J. D. Kress, R. L. Martin, D. L. Smith, N. N. Barashkov, J. P. Ferraris, *Appl. Phys. Lett.* **1997**, 71, 3528.
 [14] I. H. Campbell, S. Rubini, T. A. Zawodzinski, J. D. Kress, R. L. Martin, D. L. Smith, N. N. Barashkov, J. P. Ferraris, *Phys. Rev. B: Condens. Matter* **1996**, 54, R14321.

[15] F. Nüesch, F. Rotzinger, L. Si-Ahmed, L. Zuppiroli, *Chem. Phys. Lett.* **1998**, 288, 861.
 [16] L. Zuppiroli, L. Si-Ahmed, K. Kamaras, F. Nüesch, M. N. Bussac, D. Ades, A. Siove, E. Moons, M. Grätze, *Eur. Phys. J. B* **1999**, 11, 505.
 [17] H. Lüth, *Surfaces and Interfaces of Solid Materials*, 3rd ed., Springer, Berlin **1998**.
 [18] M. Bruening, E. Moons, D. Cahen, A. Shanzer, *J. Phys. Chem.* **1995**, 99, 8368.
 [19] S. Bastide, R. Butruille, D. Cahen, A. Dutta, J. Libman, A. Shanzer, L. Sun, A. Vilan, *J. Phys. Chem. B* **1997**, 101, 2678.
 [20] M. Bruening, R. Cohen, J. F. Guillemoles, T. Moav, J. Libman, A. Shanzer, D. Cahen, *J. Am. Chem. Soc.* **1997**, 119, 5720.
 [21] S. D. Evans, A. Ulman, *Chem. Phys. Lett.* **1990**, 170, 462.
 [22] S. D. Evans, E. Urankar, A. Ulman, N. Ferris, *J. Am. Chem. Soc.* **1991**, 113, 4121.
 [23] R. W. Zehner, B. F. Parsons, R. P. Hsung, L. R. Sita, *Langmuir* **1999**, 15, 1121.
 [24] S. B. Sachs, S. P. Dudek, R. P. Hsung, L. R. Sita, J. F. Smalley, M. D. Newton, S. W. Feldberg, C. E. D. Chidsey, *J. Am. Chem. Soc.* **1997**, 119, 10563.
 [25] L. A. Bumm, J. J. Arnold, M. T. Cygan, I. D. Dunbar, T. P. Burgin, L. Jones, D. L. Allara, P. S. Weiss, *Science* **1996**, 271, 1705.
 [26] The value of β is an average from previous studies on both conjugated and non-conjugated molecules [24,25]. Such an average is needed as our molecules have both saturated and unsaturated parts.
 [27] H. C. Card, E. H. Rhoderick, *J. Phys. D* **1971**, 4, 1589.
 [28] J. H. Werner, H. H. Güttler, *J. Appl. Phys.* **1991**, 69, 1522.
 [29] S. M. Sze, *Physics of Semiconductor Devices*, 2nd ed., Wiley, New York **1981**.
 [30] J. M. Andrews, M. P. Lepselter, *Solid-State Electron.* **1970**, 13, 1011.
 [31] R. T. Tung, *Phys. Rev. Lett.* **2000**, 84, 6078.
 [32] The image force lowering term in Equation 4 should probably also take into account the permittivity of the insulator. However, because there is no simple analytical expression to describe image force lowering through a medium with a permittivity smaller than that of the semiconductor, we use only the simple expression here. This should not significantly affect the results because of the weak (square root) dependence of the image force lowering on E_m . An exact treatment is beyond the scope of this letter. For more discussion on this topic see: a) M. Kleefstra, G. C. Herman, *J. Appl. Phys.* **1980**, 51, 4923. b) A. Tugulea, D. Dascalu, *J. Appl. Phys.* **1984**, 56, 2823.
 [33] H. K. Henisch, *Semiconductor Contacts: An Approach to Ideas and Models*, Oxford Science Publications, **1984**.
 [34] A. L. McClellan, *Tables of Experimental Dipole Moments*, W. H. Freeman and Company, **1963**.
 [35] E. Moons, M. Bruening, A. Shanzer, J. Beier, D. Cahen, *Synth. Met.* **1996**, 76, 245.

Enhanced Visible Light Conversion Efficiency Using Nanocrystalline WO₃ Films**

By Clara Santato, Martine Ulmann, and Jan Augustynski*

A common feature of semiconductors exhibiting indirect optical transition is the low magnitude of their absorption coefficient, α , that is the large penetration depth, $1/\alpha$, of photons, especially those with energies close to the bandgap. For materials, such as silicon, exhibiting large diffusion lengths for minority charge carriers, L_p (for the positive holes), the comparably large $1/\alpha$ values impose fabrication of relatively thick devices (e.g., p–n junction solar cells) in order

[*] Prof. J. Augustynski, Dr. C. Santato, Dr. M. Ulmann
 Department of Chemistry, University of Geneva
 CH-1211 Geneva 4 (Switzerland)
 Jan.Augustynski@chiam.unige.ch

[**] This work was supported by the Swiss Federal Office of Energy and the Swiss National Science Foundation. We also thank Dr. V. Shklover, Institute of Crystallography and Petrography, ETH, Zürich, for carrying out SEM analyses.

to preserve high conversion efficiencies. The situation is quite different for large bandgap oxide semiconductors, such as n-type TiO₂ or WO₃ employed in photoelectrochemical devices, having small mobilities and short hole (minority carrier) diffusion lengths.^[1–3] This implies that in such a case (and for a semiconductor with a moderate doping level), it is mainly the carriers generated within the depletion (space charge) layer that will contribute to the photocurrent. For the applications of WO₃ as a photocatalyst or a photoanode in a photoelectrolysis cell under solar light illumination, it is particularly important to maximize their response to the wavelengths close to the bandgap. This, in turn, requires the depletion layers to be wide enough to match the penetration depth of light, $1/\alpha$. To fulfil the latter condition, the depletion layer widths, W , for WO₃ should be several micrometers.^[4,5] The value of

$$W = (2\epsilon\epsilon_0(V - V_{fb})/eN_D)^{1/2}$$

where ϵ_0 is the permittivity of vacuum, V is the actual (applied) potential, V_{fb} is the flat-band potential ($V - V_{fb}$ being the band bending), and e is the charge on the electron, can be calculated from the known number of donors per cm³, N_D , and the dielectric constant of the semiconductor, ϵ . Assuming, for example, a moderate doping level $N_D = 10^{16}$ cm⁻³ and a 1 V potential drop across the depletion layer, one obtains for WO₃ ($\epsilon = 50$)^[2] a W value of 0.75 μ m. This is just enough to match, in the case of WO₃ (having bandgap energy $E_g \approx 2.5$ eV), the penetration depth of 370 nm light, significantly below the fundamental absorption edge at about 500 nm. A possible way to increase the width of the depletion layer could be to decrease the donor concentration, N_D . However, this would lead to a large ohmic drop within the semiconductor and limit again the photocurrent efficiency.

It is particularly interesting and potentially important from the practical point of view that, as described in the present communication, the nanocrystalline WO₃ photoelectrode escapes the above limitations inherent in the bulk semiconductor.

The nanoparticulate WO₃ films used in this study were obtained by depositing on conducting glass substrates, layer by layer, a colloidal solution of tungstic acid. Conducting glass plates (Libbey Owens Ford, 12 Ω /square) comprised a 0.5 μ m thick overlayer of F-doped SnO₂. The precursor (tungstic acid) was obtained by passing an aqueous solution of sodium tungstate through a column filled with a proton exchange resin (Dowex 50 WX2, 100–200 mesh). A viscous solution of tungstic acid and polyethylene glycol was applied to the substrate and then annealed in flowing oxygen at 550 °C for 30 min.^[6,7] The thickness of individual layers (as determined with a Tencor Alpha Step 200 profilometer) was close to 0.4 μ m. The WO₃ films used for most of the experiments described in this communication were about 2.5 μ m thick and were formed by six consecutive applications of the solution, each followed by the heat treatment. As shown in a typical scanning electron micrograph displayed in Figure 1, such a

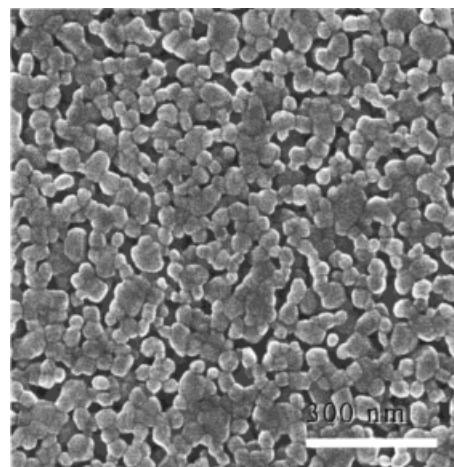


Fig. 1. Scanning electron micrograph of a 2.5 μ m thick mesoporous WO₃ film.

film is composed of WO₃ particles with diameters of a few tens of nanometers partly fused together. Owing to their mesoporous structure, WO₃ films of this kind can be penetrated by the electrolyte down to the back contact to form high-surface-area semiconductor/liquid junctions.

The bulk WO₃ electrodes were prepared by oxidizing tungsten metal in flowing oxygen at 750 °C,^[8] followed by a photoelectrochemical activation treatment.^[9]

The photoelectrochemical measurements were carried out in a two-compartment Teflon cell equipped with a quartz window, by illuminating the WO₃ electrode from the front (i.e., film/solution interface). The potential of the WO₃ electrode was monitored versus a mercurous sulfate–mercury reference electrode and is quoted versus the reversible hydrogen electrode (RHE) in the same solution.

Figure 2 compares photocurrent–potential plots for a nanocrystalline and a bulk WO₃ electrode illuminated with two different wavelengths, 380 and 440 nm. (To make the comparison easier, the photocurrents were divided by the product of the incident photon flux and of the electron charge, i_{ph}/Φ_e ,

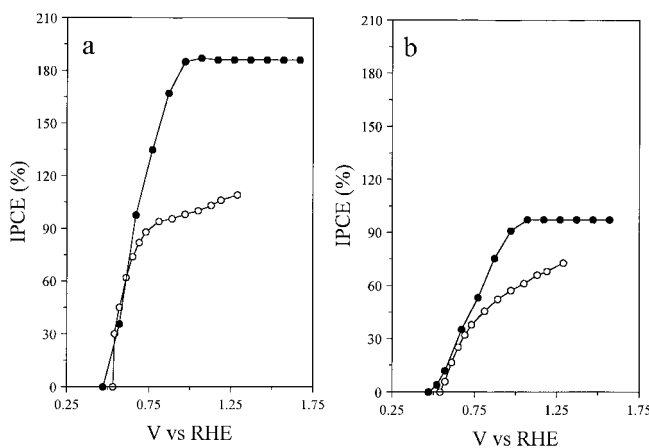


Fig. 2. Incident photon-to-current conversion efficiency–potential curves for a nanocrystalline (about 2.5 μ m thick) and a bulk WO₃ photoelectrode (filled and open circles, respectively) recorded in a 0.1 M CH₃OH/1M H₂SO₄ solution: a) under 380 nm illumination from a 500 W Xe lamp equipped with a monochromator; b) under 440 nm illumination.

and are presented as the incident photon-to-current conversion efficiencies, IPCE). The holes generated by the absorbed light oxidize methanol preferentially, a reaction known to involve photocurrent doubling, which explains the IPCE values close to 200%.^[10] Even if the penetration depth of the 380 nm light in the bulk WO₃ is of the order of 1 μm, it apparently already exceeds the collection distance of the minority carriers within the semiconductor given by the sum of W and L_p .^[11] This is consistent with the observed continuing increase of IPCE with increasing the applied potential (i.e., the band bending). In contrast, for the nanocrystalline photoanode, the photocurrent reaches a saturation level, corresponding to an almost ideal IPCE of about 190%, already in the presence of an about 0.5 V potential difference. As the absorption coefficient of the 380 nm light in the nanocrystalline WO₃ film is similar to that earlier reported for the bulk WO₃,^[12] the much higher photocurrent efficiency observed for the former material must be related to a different mechanism of charge separation.

The fact that the observed efficient charge separation in the nanocrystalline WO₃ electrodes cannot be assigned to the presence of a conventional space charge (depletion) layer is clearly confirmed by the IPCE–potential plots obtained under 440 nm illumination, displayed in Figure 2b. Despite a much larger optical penetration depth in the semiconductor than for the 380 nm light, in the case of the nanocrystalline electrode the saturation photocurrent is attained again after application of a about 0.5 V potential difference. On the other hand, the continuous steep rise of the photocurrent recorded for the bulk electrode reflects the essential role of the band bending in matching (via the increased width of the depletion layer) the light penetration depth.

The mechanism of separation of photogenerated charge carriers as well as the charge transport in the nanocrystalline semiconductor films is the subject of continuing discussion.^[13] From analogy with the concepts used to describe the behavior of suspended colloidal particles,^[14] it was suggested that the charge separation in the nanocrystalline films is also controlled by the charge transfer kinetics to the redox species in the solution.^[15] This implies that, in order to collect efficiently the electrons at the back contact of the film, the forward charge transfer (i.e., in the case of an n-type semiconductor, the oxidation of the solution species by the valence band holes) has to be not only much faster than the reverse reaction, but, more generally, faster than any process of electron transfer to the acceptor species present in the solution. The latter condition is actually fulfilled for the photooxidation of methanol at WO₃: a rather irreversible reaction. The fact that, regardless the penetration depth of the incident light, the potential difference to be applied to the nanocrystalline electrode, in order to reach the saturation photocurrent, is practically constant, on the order of 0.5 V (compare Fig. 2) shows clearly that it can not be identified with the band bending in any kind of space charge layer formed in a part of the nanocrystalline film. However, a potential drop is expected to exist at the back contact (i.e., at the SnO₂–F/WO₃ interface) as well

as across the Helmholtz layer being formed at the interface between the network of WO₃ nanoparticles and the solution.^[16,17]

One of the consequences of the moderate bias required by the nanocrystalline electrodes is that the photocurrent efficiency for the wavelengths close to the band edge can be increased simply by adapting the thickness of the semiconductor film. This is particularly important in view of the applications of a WO₃ photoanode to the photoelectrolysis of water and to the photodegradation of organic effluents since the solar light intensity strongly increases through the 400–500 nm wavelength region.

A marked effect of the nanocrystalline film thickness upon the photocurrent efficiency is illustrated in Figure 3 for a series of WO₃ electrodes consisting of the increasing number of deposited layers. These data were recorded at a potential of 1 V vs. RHE (i.e., about 0.5V above the onset potential of the

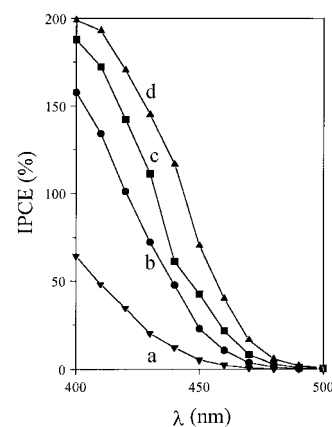


Fig. 3. Spectral photoresponses for a series of nanocrystalline WO₃ electrodes, having different thicknesses: a) about 0.4 μm, b) 1.2 μm, c) 2.5 μm, and d) 4 μm, recorded in the 400–500 nm range of wavelengths, close to the absorption edge, 0.1 M CH₃OH/1 M H₂SO₄ solution, applied potential, 1 V vs. RHE.

photocurrent), in the case of methanol oxidation, but the same trend was also observed for the photooxidation of water. Importantly, another nanocrystalline semiconducting oxide TiO₂ exhibits a behavior closely similar to that of WO₃. For example, in the case of photooxidation of formic acid at the nanocrystalline TiO₂ anode, the saturation photocurrent is reached about 0.4 V above the onset potential both under the short-wavelength (300 nm) and the 380 nm (close to the absorption edge) illumination.^[18]

The results described in this report confirm a totally different mechanism of charge separation in a nanocrystalline oxide semiconductor as compared to its bulk analogue. While in the latter case, the large optical penetration depths close to the absorption edge can be only (at least, in part) matched by the increased anodic bias, for the nanocrystalline WO₃ electrode the saturation photocurrent is attained under a moderate, constant bias regardless the incident light wavelength. This explains in particular a large improvement in solar conversion efficiency observed for the mesoporous WO₃ electrodes.

Received: September 18, 2000
Final version: December 20, 2000

- [1] The hole diffusion length in the bulk WO_3 estimated by Butler [2] is about 0.15 μm .
- [2] M. A. Butler, *J. Appl. Phys.* **1977**, *48*, 1914.
- [3] A. K. Ghosh, H. P. Maruska, *J. Electrochem. Soc.* **1977**, *124*, 1516.
- [4] According to the data reported by Deb [5], the optical penetration depths ($1/\alpha$) in crystalline WO_3 are about 2.2 μm at 420 nm, and 4.5 μm at 440 nm, respectively.
- [5] S. K. Deb, *Philos. Mag.* **1973**, *27*, 801.
- [6] Patent pending PCT/CH 99/00270.
- [7] C. Santato, M. Ulmann, J. Augustynski, presented at *IPS-2000: 13th International Conference on Photochemical Conversion and Storage of Solar Energy*, Snowmass, CO, July 30–August 4 **2000**.
- [8] W. Gissler, R. Memming, *J. Electrochem. Soc.* **1977**, *124*, 1710.
- [9] M. Spichiger-Ulmann, J. Augustynski, *J. Appl. Phys.* **1983**, *54*, 6061.
- [10] S. R. Morrison, T. Freund, *J. Chem. Phys.* **1967**, *47*, 1543.
- [11] The actual donor density in the bulk WO_3 is larger than that used in the example calculation, of the order of 10^{17} – 10^{18} cm^{-3} .
- [12] Our preliminary absorbance measurements performed with nanocrystalline WO_3 films deposited on quartz substrate (C. Santato, R. Dhre) indicate slightly lower absorption coefficients than those reported in [5].
- [13] A. Hagfeldt, M. Grätzel, *Acc. Chem. Res.* **2000**, *33*, 269.
- [14] M. Grätzel, in *Photocatalysis, Fundamentals and Applications* (Eds: N. Serpone, E. Pelizzetti), Wiley, New York **1989**, p. 123.
- [15] A. Hagfeldt, M. Grätzel, *Chem. Rev.* **1995**, *95*, 49.
- [16] G. Schlichthörl, S. Y. Huang, J. Sprague, A. Frank, *J. Phys. Chem. B* **1997**, *101*, 8141.
- [17] A. Zaban, S. Ferrere, B. Gregg, *J. Phys. Chem. B* **1998**, *102*, 452.
- [18] A. Wahl, J. Augustynski, *J. Phys. Chem. B* **1998**, *102*, 7820.

Dense Nanostructured t-ZrO₂ Coatings at Low Temperatures via Modified Emulsion Precipitation**

By Fiona C. M. Woudenberg, Wiebke F. C. Sager, Natascha G. M. Sibelt, and Henk Verweij*

Research on the preparation and characterization of nanocrystalline material with average grain sizes well below 100 nm has increased tremendously over the last two decades and its application in new technologies is manifold. Captivating properties resulting from the large surface/volume ratio make them not only interesting as novel bulk materials but also for coatings and composite materials. Besides recent innovative utilization as antifogging and self-cleaning coatings,^[1] there exists an enormous demand for protective ceramic coatings against corrosion, heat, or wear on a variety of different materials, such as metal, plastic, or even textile. This requires the development of new techniques that allow the

application of nanostructured coatings (grains < 20 nm) of high-melting oxides at very low temperatures (< 200 °C) and costs. In this communication we describe the preparation of dense nanostructured tetragonal ZrO_2 coatings with grain sizes of 10 nm after low-temperature treatment. Essential in this approach is the controlled preparation, crystallization, and densification of non-agglomerated ZrO_2 nanoparticles of 5–8 nm via modified emulsion precipitation. The method developed opens up the possibility of applying nanocoatings of high-melting oxides at temperatures low enough for coating steel or plastic.

Special attention has recently been paid to nanostructured high-melting oxide ceramics, such as tetragonal zirconia (t- ZrO_2). They are particularly suitable as wear-resistant insulating coatings on, for example, superalloy engine parts, offering (hot) corrosion and thermal shock protection due to their high chemical inertness, low thermal conductivity, and relatively large thermal expansion coefficient.^[2,3] Homogeneous mono- or multilayers of nanocrystalline zirconia with grain sizes below 20 nm have so far only been prepared by reactive sputter deposition techniques^[4] or classical sol-gel techniques in combination with adsorption onto self-assembled monolayers in the early stages of particle precipitation.^[5] Direct coating of substrates from particle suspensions is possible if the nanoparticles obtained are < 10 nm in size, not agglomerated, and easy to pack into dense layers. This would result in a greatly reduced densification/sintering temperature and minimal grain growth.^[6] ZrO_2 particles < 10 nm in size obtained by sol-gel based processes are generally highly agglomerated^[7] and more elaborate methods for obtaining monodisperse ZrO_2 did so far not result in particle sizes < 30 nm.^[8] To obtain non-agglomerated nanoparticles, precipitation reactions have also been performed in heterogeneous media, such as emulsions, micellar systems, and microemulsions using the interior of the dispersed phase as isolated nanoreactor.^[9,10] Oxide precursor particles can generally be prepared by dispersing the metal ion-containing aqueous phase in a non-polar medium (oil), whereby hydroxide formation can be induced by an increase in pH and/or removal of water. Problems encountered during the preparation of nano- ZrO_2 via (micro)emulsion precipitation are growth of particles beyond the dimensions of the droplet micro-/nanoreactors and strong and uncontrolled aggregation, especially during the water removal step.^[11]

The aim of this study was the preparation of well-defined dense nanostructured oxide coatings consisting of t- ZrO_2 grains < 20 nm at rather low temperatures by deposition of nanoparticles synthesized via a modified emulsion precipitation method. To prepare such coating layers by deposition of colloidal nanoparticles, it is a prerequisite to start with completely agglomerate-free particle dispersions with an average particle size below 10 nm that can pack into random close-packed mono- or multi-layers with minimal shrinkage and grain growth during subsequent combined calcination and densification steps. The method developed allows integrated particle handling without separate particle drying and calcina-

[*] Prof. H. Verweij, F. C. M. Woudenberg, N. G. M. Sibelt
Laboratory of Inorganic Materials Science, MESA⁺ Research Institute
University of Twente
PO Box 217, NL-7500 AE Enschede (The Netherlands)
E-mail: H.Verweij@ct.utwente.nl

Dr. W. F. C. Sager
Membrane Technology Group, Faculty of Chemical Technology
University of Twente
PO Box 217, NL-7500 AE Enschede (The Netherlands)

[**] The authors thank The Netherlands Science Foundation (NWO-CW, PPM) and The Netherlands Technology Foundation (STW) for financial support. We are grateful to R. Keim (MESA⁺, University of Twente), F. G. Holthuysen (Philips Research), and H. Schönherr (MTP, University of Twente) for performing the electron and atomic force microscopy measurements.